A Path Integral Investigation and Numerical Simulation of the Two-Slit Problem in Quantum Mechanics

A Senior Thesis

by

Daniel Cernak

Submitted in partial fulfillment of the requirements for

the degree of Bachelor of Science with Honors

from the University of Michigan Physics Department,

College of Literature, Science, and the Arts

Department of Physics

University of Michigan - Ann Arbor

April 2024

Advisor: Professor Dante Amidei

Table of Contents

List of Figures

Abstract

In this paper we describe a complete numerical treatment of the two-slit experiment for quantum mechanics. We first introduce the two-slit problem and the Fraunhofer approximation. We describe a number of experimental approaches, including the experiment of F. Shimizu, K. Shimizu, and H. Takuma in which they subject ultracold neon atoms to the two-slit experiment. We then present the Feynman Path Integral Method and its application to the two-slit problem. Using this method, we create a toolkit to simulate this experiment, before expanding this program. We explore the visualizations created by our program, and we compare the behaviors of particles simulated in different experiments and compare the behaviors to the Fraunhofer approximation. Finally, we note how this program can then be used to simulate a variety of particles and initial conditions and their subsequent behaviors with different gratings in both the near and far regions.

1. The Two-Slit Problem in Optics

In 1802, Thomas Young performed his famous Double-Slit experiment displaying the wave nature of light [1]. In this experiment, light spreads out from a source point and falls on a plane with two closely spaced holes, which become two coherent sources of light whose interference can then be observed on a screen. The resulting irradiance interference pattern produces alternating maxima and minima of different magnitudes, with the locations of the maxima depending on the spacing of the slits, the location of the observing screen, and the wavelength of the light, demonstrating that light is a wave [1].

The treatment of the two-slit experiment reveals three regions in which the resulting interference behaves differently. The setup for the treatment is shown in Figure 1. The slit separation, as measured from their centers, is *a*. The width of each slit is *b*. First, when the observation screen is very close to the apertures, the behavior is characterized by geometric optics, in which the light is treated as rays instead of waves [1]. Here, the pattern is a sharp image of the slits. Second, when the screen is far from the aperture, the interference is described by Fraunhofer diffraction and appears as a pattern of regularly alternating light and dark fringes of varying intensity. The irradiance, I, of the light traveling through the slits at a point on the screen is given by Eq. (1a) [1].

$$I \propto \left(\frac{sin\beta}{\beta}\right)^2 cos^2\alpha \tag{1a}$$

where,

$$\beta = \frac{1}{2} kb\, sin\theta \tag{1b}$$

$$\alpha = \frac{1}{2} ka\, sin\theta \tag{1c}$$

In Eqs. (1a-c), *a* is the separation between the centers of the slits, *b* is the width of the slits, *k* is the wave number of the light, and *θ* is the angle between the line normal to the plane of the slits and the line from the middle of the wall between the slits to the point on the screen. A diagram of the Fraunhofer pattern is also given in Figure 1.

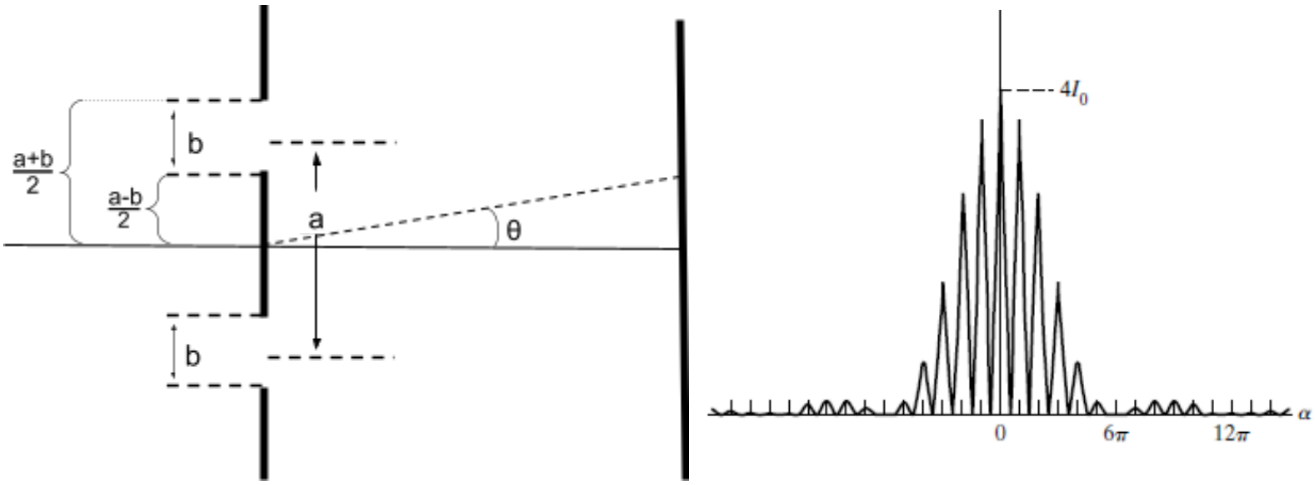

Fig. 1. *Left*: Two-slit experiment setup and measurements from Ref. [1]. *Right*: Fraunhofer two-slit pattern given by Eq. (1a) from Ref. [1].

This Fraunhofer region lies at distances *d* satisfying Equation (2):

$$Fraunhofer\colon\ d \gg \frac{a^2}{\lambda} \tag{2}$$

where λ is the wavelength of the light [1]. When the screen is closer to the slits than this distance, we lie within the third region, known as the Fresnel region. In this case, either the source or the observation screen, or both, are close enough to aperture that the estimations of Fraunhofer diffraction cannot be accepted. Fresnel diffraction acts as "a continuity between the patterns characterizing geometrical optics at one extreme and Fraunhofer diffraction at the other" [1]. The interference pattern in the Fresnel region is described as an image of the apertures, but with the edges fringed [1].

2. The Two-Slit Problem in Quantum Mechanics

Over 120 years after Young's experiment demonstrated the wave nature of light, Louis de Broglie proposed that particles could behave as waves as well. He went as far as to postulate that a particle moving at a speed *v*, with a mass *m*, would have a wavelength *λ* given by Equation (3), where *p=mv* is the momentum, and *h* is Planck's constant [2].

$$\lambda = \frac{h}{p} = \frac{h}{mv} \tag{3}$$

If particles did behave as waves, the two-slit experiment could then be conducted on particles with the expectation that the same interference pattern would arise as for light, but with the wavelength being replaced by the de Broglie wavelength.

In 1927 Clinton Davisson and Lester Germer directed a beam of electrons against a nickel target and measured the intensity of the scattered beam in various directions in front of the target [3]. A similar setup is depicted in Figure 2. Initially, the sample was polycrystalline, consisting of numerous randomly oriented microscopic crystals, causing the beam to be reflected diffusely. This meant that the intensity followed a smooth distribution. After an accident occurred, the nickel had to be baked in a high-temperature oven which created large regions of continuous crystal planes, effectively creating one large crystal of nickel. When the experiment was repeated, strong maxima of intensity were observed at specific angles. The positions of these maxima depended on the accelerating voltage applied to the electrons [2].

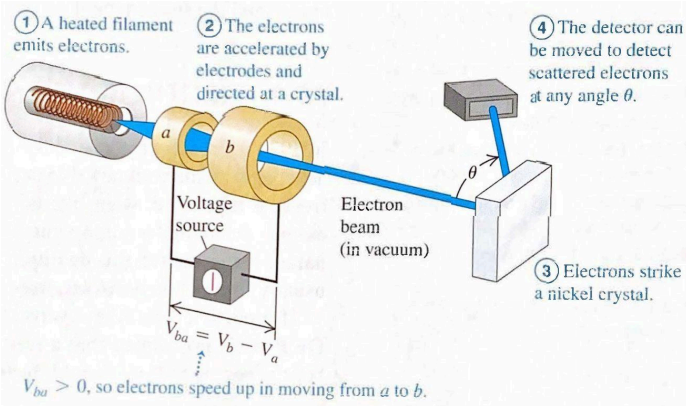

Fig. 2. An apparatus similar to that used by Davisson and Germer to discover electron diffraction from Ref. [2].

Fifteen years before, Max von Laue and others performed an experiment demonstrating the interference patterns resulting from x-rays being scattered off of a crystal [2]. As x-rays collide with the crystal, they induce electric dipole moments in the atoms. These dipoles then emit the scattered waves at different phases than each other. In order for radiation to reach an

observer from the entire array of atoms in phase, two conditions have to be met. The first is that the angle of incidence for the wave impinging on the atoms must equal the angle of the scattering, θ. The second condition, known as the Bragg condition, is that the difference in the length of the path between the source and the observer that the scattered waves travel by for adjacent rows of atoms must be an integer multiple of the wavelength of the x-rays [2]. This condition can be summarized by Equation (4),

$$2d\ sin(\theta) = m\lambda,\ (m = 1, 2, 3,\ldots) \tag{4}$$

where d is the distance between adjacent rows in the array [2]. When both conditions are satisfied, there is a strong maximum in the interference pattern. These x-ray diffractions were used to verify that x-rays are waves, and can be used to determine the wavelength of x-rays [2].

Davisson and Germer noticed the similarities between the behavior of their electron beams and the x-ray diffraction. From the accelerating voltage, they could determine the speeds of the electrons and thus their momenta, and then use Eq. (3) to obtain the de Broglie wavelength for the electrons [2]. Davisson and Germer then used x-ray diffraction to solve for the distance between adjacent atoms in the nickel. Using the Bragg condition for the crystal and the de Broglie wavelength for λ, they found the expected diffraction angles agreed with their observed angles. Thus, Davisson and Germer discovered electron diffraction, the first and very direct experimental confirmation of De Broglie's hypothesis for the wave behavior of matter [2]. Since it had now been shown that particles do behave like waves, the two-slit experiment could now be conducted on particles.

In 1961 Claus Jönsson became the first person to perform the double-slit experiment with electrons [4]. Other experiments had been performed observing the diffraction and interference of electrons in different setups, but his report investigated the diffraction of electron waves at arrangements of a single slit up to five slits. The electrons in the experiment were accelerated through 50 kV and had a de Broglie wavelength of 0.05 Å. This small wavelength made it impossible to create slits in solid material that were on the order of the wavelength. His

slits were created by irradiating a silver covered glass plate by a line-shaped electron probe. This process created a layer of polymerized hydrocarbon at the locations of high electron current density. When a copper layer is then electrolytically deposited, these areas are left free of copper. Peeling the copper layer away, then gives a copper foil with slits free of any material [4]. The slits used were 50 μm long and 0.5 μm wide, with a spacing of 2 μm. Electrons were then emitted by the source and passed through a circular aperture and two electrostatic cylinder lenses, which created a line-shaped source to illuminate the slits. The diffraction pattern from the slits was projected onto an observation plane 350 mm after the slits. Lenses and a long exposure camera were then used to magnify and record the diffraction pattern. The patterns were then compared to the theoretical expectations of the Fraunhofer diffraction pattern. The locations of the maxima and minima agreed qualitatively, and any deviation was attributed to the finite widths of the slits [4]. Thus, Jönsson displayed how the diffraction of a beam of electrons in the two-slit experiment produced the same pattern as for a beam of light in the Fraunhofer region, as expected from de Broglie.

In 1974 Pier Giorgio Merli, Gian Franco Missiroli, and Giulio Pozzi expanded upon the two-slit diffraction with electrons, by using single electrons, rather than a beam [5]. They explained that the interference pattern observed is the sum of the independent events of each electron interacting with the slits. While this fact was proposed from previous calculations in other experiments, this experiment displayed the result with direct observation [5]. They used a hot filament and condenser lenses to create a monochromatic source of electrons. They then replaced the photographic plate used to view the impact of the electrons with an image intensifier that creates an image 200 times brighter. The image is then transmitted to a television monitor. This setup allows for the observation of very low intensities, even down to one electron at a time, seen as a white dot on the television monitor. They could then observe one electron arriving at a time and the overall resulting distribution. After thousands of electrons arrived, the usual fringes began to appear. The experiment displayed that “every electron hits the television

monitor at a precise spot, like a particle ... but the cumulative behavior of many electrons (even when they are transferred one by one from the emitting filament to the television monitor) shows a wave-like pattern" [5]. The experiment demonstrated that electrons are neither waves nor particles only, but behave as both at different times. It also further confirmed that the interfering behavior occurs from the single electron itself, and not from its interference with other electrons in a beam [5]. More recent experiments with electrons have corroborated these findings [6]. Finally, the experiment also demonstrated that the probability of an electron impacting the observation screen at a specific point can be estimated by counting the number of electrons that impacted the screen in an area around the point and comparing that to the total number of electrons reaching the screen [7].

Then, in 1992, Fujio Shimizu, Kazuko Shimizu, and Hiroshi Takuma performed the double slit experiment, not on electrons, but on ultracold neon atoms [8]. The benefit of using cold atoms is that a colder and slower atom has a longer de Broglie wavelength, Eq. (3), reducing the accuracy required of the components and allowing the use of an interferometer on the same scale as optical interferometers. Using atoms also investigates whether the wave description can be applied to a larger and more complex object like an atom. In this experiment, the atoms used were ultracold neon atoms, around 2.5 mK, which were trapped in a magneto-optical trap and then allowed to fall due to gravity. Gravitational acceleration was used to move the atoms because they are neutral. As the atoms fell, they interacted with a pair of slits 76 mm below the trap, and collided with a fluorescent plate 113 mm below the slits. The double slits had openings of 2 μm and a spacing of 6 μm. The resulting images on the plate were amplified by an image intensifier and detected by a CCD camera as a video. The video frames at different times then showed the images produced by atoms of different initial velocities. Atoms that collided with the plate earlier would have had an initial downwards velocity in order to reach the plate quicker. The interference patterns at different times were then compared with each other and with the theoretical Fraunhofer curve for atoms with zero initial velocity and a

plate collision at 196 ms. When this was compared to the experimental curve of the same collision time, the estimated fringe separation agreed well with the experimental separation. Similarly, the variation in the fringe separation with time agreed with the theoretical value [8]. This experiment demonstrated the two-slit interference pattern for atoms accelerated by gravity instead of electrons of nearly constant velocity, and the results again agreed with the expectations given by de Broglie and Fraunhofer, further demonstrating the wave nature of matter.

3. Calculating the Two-Slit Interference Pattern

While the experimental application of the two-slit problem to electrons and atoms confirmed the wave-like behavior of matter suggested by de Broglie and agreed with the Fraunhofer estimation, calculational methods can also be used to learn more about the behavior of matter subjected to the two-slit experiment, especially outside of the Fraunhofer region, and to create expectations for future experiments. The first and most typical of these calculations is the Fraunhofer estimation because of its relative ease. The Fraunhofer estimation, described earlier, is given by Eq. (1). The calculation only requires the dimensions of the slits, the wavelength of the light or particles, and the distance between the slits and the screen and is able to produce an analytic solution for the distribution of the irradiance or probability, making it an easy choice for calculations. The Fraunhofer distribution; however, is an approximation assuming that both the source and screen are sufficiently far from the slits, at a distance greater than $\frac{a^2}{\lambda}$ as given by Eq. (2), with *a* being the separation of the slits [1]. When this is not the case, the estimation becomes worse, eventually becoming unusable when either are close enough. Ultimately, the Fraunhofer estimation is very useful for calculating expectations within its regime, but in order to further investigate the behavior of the two-slit experiment, other methods are needed.

Moving closer than the Fraunhofer distribution into the Fresnel region, one solution proposed in the field of optics is the Fresnel-Kirchhoff diffraction formula given by Equation (5) [1].

$$E_P = \frac{-ikE_S}{2\pi} e^{-i\omega t} \int\int F(\theta) \frac{e^{ik(r+r')}}{rr'} dA \tag{5}$$

This formula produces the amplitude of the electric field at a point *P*, given by E_P, by integrating products involving exponentials, the amplitude at the source E_S, the wave number *k*, the frequency ω, time *t*, and the distances between the aperture and the source and between the aperture and *P*, given by *r* and *r'*. The integral also includes an obliquity factor *F(θ)* and is integrated over the aperture or slit. This integration still involves approximations and is generally difficult to carry out. Fresnel offered methods to simplify or avoid this integration, but these only apply in specific cases [1]. In order to obtain a method of calculation that can be applied more generally, we instead turn to work performed in the field of quantum physics.

Turning to the quantum mechanical two-slit problem, we know that the solutions must satisfy the Schrödinger Equation. One method of finding distributions that satisfy this equation is the Feynman Path Integral Method [9]. An early application of the path integral method to the two-slit problem is Ref. [10]. This method has also been numerically applied to the Shimizu experiment in order to obtain the probability distribution of the atoms [11]. This numerical method builds up the interference pattern one point at a time, rather than producing an analytic expression like the Fraunhofer method. However, the Feynman Path Integral Method has also been analytically applied to the two-slit experiment [12]. These applications were all different ways of applying this method to the two-slit problem in order to obtain an interference pattern for the particles after they traveled through the slits, both in the near and far regions.

Other methods beyond the Feynman Path Integral have also been adapted from different fields of physics. The Finite-Difference Time-Domain method has been adapted from computational electrodynamics to simulate a two-dimensional Gaussian wave packet interacting

with the two-slit experiment [13]. Similarly, the Crank-Nicolson method, typically used for the heat equation, has also been used to simulate and animate the interaction of a two-dimensional wave packet with the two-slit setup [14]. These are two examples of other methods that have been applied to the quantum two-slit problem. The goal of this paper is to establish a numerical toolkit that can be used to investigate the two-slit interference pattern outside the Fraunhofer region and can be used to explore future experimental treatments and setups. We will follow the methods of Ref [11] in the development of a robust Python based framework to numerically apply the Feynman Path Integral Method to the Shimizu experiment. We will then generalize the framework to allow for the simulation of different setups including changes in the positions of the slits, changes in the types of particles, and the choice of gravitational acceleration or a constant velocity of the particles. This generalization will turn the framework into an adjustable toolkit to be used to explore possible new experiments and create expectations for the resulting behavior.

3.1. The Feynman Path Integral Method

In quantum mechanics, the probability of an event occurring at a point *x* is denoted by *P(x)*. This probability is given by taking the absolute square of a complex quantity, called the probability amplitude, denoted by *φ(x)* [9]. If there are multiple contributions to the probability of an event, for example, two slits that an electron could travel through, the probability is not the sum of the individual probabilities, but rather the probability amplitude is the sum of the individual amplitudes [9]. These rules are summarized by the following equations from Ref. [9].

$$P = |\varphi|^2 \tag{6}$$

$$\varphi = \varphi_1 + \varphi_2 \tag{7}$$

$$P_1 = |\varphi_1|^2 \ , \ P_2 = |\varphi_2|^2 \tag{8}$$

If two possibilities, or alternatives, are exclusive however, then their probabilities will simply add. Alternatives are said to be exclusive if there is a way to unambiguously determine

which one has occurred. An example of exclusive probabilities would be the locations of the impact of electrons onto a screen of individual detectors in the two-slit experiment. For the electron detectors, the probability of an electron arriving at either of two specified detectors is the sum of their individual probabilities [9]. Since we cannot unambiguously determine which slit an electron passes through without impacting the experiment, the alternatives of the two slits are not exclusive and thus follow Eqs. (6-8).

As previously stated, the amplitude for an event is the sum of the amplitudes of the contributions. This means that the amplitude of an event is the sum of the amplitudes of the different ways that an event could take place. If we consider a particle traveling between two points in a given amount of time, we can conceive of many different paths that it could take. Since each of these possible paths contributes to the probability of the particle traveling between the two points, and since we cannot know which path was taken without interfering with the motion of the particle, these different paths represent non-exclusive alternatives. Thus, the total amplitude of the travel of the particle is the sum of the amplitudes associated with each possible path. As more paths become available and form a continuum, the summation becomes an integral of amplitudes over the possible paths [9].

For a particle moving in one dimension, the path can be described by its position as a function of time, *x(t)*. If the particle moves from the position x_a at a time t_a to a position x_b at time t_b, then we can define an amplitude, called the kernel, denoted by *K(b,a) [9]*. This amplitude is the sum of the amplitudes over all the possible trajectories between x_a and x_b in the associated time frame [9].

In classical mechanics there exists a quantity *S*, called the action, that can be calculated for any path between two points. A particle then travels between these points by following a specific path, called the classical trajectory $\bar{x}(t)$, for which the action is an extremum. Equation (9) gives the expression for the action in terms of the lagrangian, *L*, and Equation (10) gives the lagrangian for a particle with mass *m* in a potential *V(x,t)* [9].

$$S[b,a] = \int_{t_a}^{t_b} L(\dot{x}, x, t)dt \tag{9}$$

$$L = \frac{m}{2}\dot{x}^2 - V(x,t) \tag{10}$$

It is important to note that all paths, not just $\bar{x}(t)$, contribute equal magnitudes to the total amplitude, but with different phases. The phase of a path's contribution is the action along the path, in units of ħ, the reduced Planck's constant. Thus, *K(b,a)* is given by Equations (11) and (12) below [9]. The constant is chosen to normalize *K*.

$$K(b,a) = \sum_{paths\ from\ a\ to\ b} \varphi[x(t)] \tag{11}$$

$$\varphi[x(t)] = constant * e^{(i/\hbar)S[x(t)]} \tag{12}$$

In order to construct the summation in Eq. (11), we choose a subset of all the paths by dividing time into steps of width *ε*. At each time step t_i, we can then select a point x_i and construct a path by connecting these points with straight lines. The sum over all paths is then defined, in Equation (13), to be the multiple integral over all the values of x_i for *i* between 1 and *N*-1, with *N* being the number of time steps [9].

$$K(b,a) \sim \int \ldots \int\int \varphi[x(t)]dx_1 dx_2 \ldots dx_{N-1} \tag{13}$$

This integral does not include the endpoints x_0 or x_N since those points are fixed. In order to obtain a more representative sample of the infinite possible paths between the endpoints, we can make *ε* smaller, thus creating more time steps and more points to integrate over, allowing for more possible paths. The normalizing factor for Eq. (13) in the situation described for Eq. (10) is given by Feynman and Hibbs to be A^{-N}, where N is as above [9].

$$A = \left(\frac{2\pi i\hbar\varepsilon}{m}\right)^{1/2} \tag{14}$$

Thus, we now have the amplitude for a particle to move from x_a at a time t_a to x_b at time t_b, given by Equation (15) [9].

$$K(b,a) = \lim_{\varepsilon \to 0} \frac{1}{A}\int \dots \int \int e^{(i/\hbar)S[b,a]} \frac{dx_1}{A}\frac{dx_2}{A} \cdots \frac{dx_{N-1}}{A} \tag{15}$$

Since we have used an approximation in the above definition, Eq. (15) might not always be the best definition, so the sum over all paths is often written in a less specific form as:

$$K(b,a) = \int_a^b e^{(i/\hbar)S[b,a]} Dx(t) \tag{16}$$

where *Dx(t)* acts as a stand-in for a specific method of performing the integral [9].

If we now suppose that there is some time t_c between t_a and t_b then the action along any path between *a* and *b* can be written according to Equation (17).

$$S[b,a] = S[b,c\} + S[c,a] \tag{17}$$

This summation is allowed because of the definition of the action as an integral in time, and because *L* only depends on position and velocity, and no higher derivatives [9]. We then use Eq. (16) to expand the kernel, *K*.

$$K(b,a) = \int_a^b e^{(i/\hbar)S[b,a]} Dx(t) = \int_a^b e^{(i/\hbar)(S[b,c\}+S[c,a])} Dx(t) \tag{18}$$

Any path between *a* and *b* can be split into two parts. The first has endpoints x_a and x_c; the second, x_c and x_b. We can first integrate over all the paths between *a* and *c*, which leaves *S[b,c]* constant, and then integrate over all possible points of x_c [9].

$$K(b,a) = \int_{-\infty}^{\infty} \int_c^b e^{(i/\hbar)S[b,c]} K(c,a) Dx(t) dx_c \tag{19}$$

Then, we can integrate over all the paths between the arbitrary x_c and the point x_b, leaving an integral over x_c [9].

$$K(b,a) = \int_{-\infty}^{\infty} K(b,c)K(c,a)dx_c \tag{20}$$

From here we can make three conclusions. First, we can conclude that the kernel to go from point *a* to point *b* can be found by taking the amplitude for the particle to go from point *a* to point *b*, by way of point *c*, and summing over all possible positions of point *c*. This method sums

over all of the paths from *a* to *c* and from *c* to *b* and then repeats this process for all points that *c* could be, effectively summing over all the paths from *a* to *b*. Thus, this method mirrors our definition from Eq. (11). From this conclusion, along with Eq. (20), we can see that the amplitude to go from point *a* to point *b*, by way of point *c,* is simply the kernel to go from *a* to *c* times the kernel to go from *c* to *b*. These then lead to our final conclusion: the overall amplitude for events occurring in succession in time is the product of the individual amplitudes of the events [9].

In quantum mechanics, often the point of interest in a problem is the wave function, Ψ, a complex function of space and time. This wave function is often obtained by solving the Schrödinger Equation:

$$i\hbar\frac{d\Psi}{dt} = \left(-\frac{\hbar^2}{2m}\nabla^2 + V\right)\Psi \tag{21}$$

The interpretation of Ψ is that its absolute square gives the probability of finding a particle at a specific point in space at a specific time. In the one dimensional case this is given by Equation (22) [15].

$$\int_a^b |\Psi(x,t)|^2 dx = \textit{\{probability of finding the particle between a and b, at time t\}} \tag{22}$$

Since the absolute square of Ψ is a probability function, Ψ is then a probability amplitude, like φ in Eq (6). We can then conclude, since Ψ is an amplitude, that it satisfies the rules for the combination of amplitudes that we described above [9]. Thus, we can multiply the wave function at a specific location and time (x_a,t_a) by the kernel representing the movement of the particle to a new location and time (x_b,t_b) to obtain a new amplitude whose absolute square represents the probability of the particle to be initially at x_a and move to x_b at time t_b [9]. Similarly to Eq. (20), if we now integrate this product over all of the locations where Ψ is defined, we will then obtain the amplitude for the particle described by Ψ at t_a to be at x_b at time t_b [9].

$$\Psi\left(x_b, t_b\right) = \int_{-\infty}^{\infty} K(b,a)\Psi\left(x_a, t_a\right)dx_a \tag{23}$$

As Eq. (23) shows, the total amplitude to arrive at (x_b,t_b), is the sum, over all possible values of x_a, of the total amplitude at the point (x_a,t_a), that is, $\Psi(x_a,t_a)$, multiplied by the amplitude to go from *a* to *b*, $K(b,a)$ [9]. This means that by using this method, we can propagate an initial wave function through time, as long as we can calculate the kernel.

The Lagrangian for a free particle is that of Eq. (10), with the potential term, V, set equal to zero at all points. Using Eqs. (9,14,15), the kernel for a free particle, K_0 is given by Equation (24) [9].

$$K_0(b,a) = \lim_{\varepsilon \to 0} \left(\frac{m}{2\pi i\hbar\varepsilon}\right)^{N/2} \int \dots \int exp\left\{\frac{im}{2\hbar\varepsilon}\sum_{n=1}^{N}\left(x_n - x_{n-1}\right)^2\right\} dx_1 \dots dx_{N-1} \tag{24}$$

Once the gaussian integrals are completed and the limit is taken, K_0 becomes [9]:

$$K_0(b,a) = \left(\frac{m}{2\pi i\hbar(t_b - t_a)}\right)^{1/2} exp\left\{\frac{im(x_b - x_a)^2}{2\hbar(t_b - t_a)}\right\} \tag{25}$$

With this free particle kernel we can now propagate a wave function through time in free space. The goal of this thesis is to use this path integral method to solve for the interference pattern in a real two-slit experiment. In Section 4 we outline the experiment, and in Section 5 we describe the calculation.

4. The Shimizu Experiment: A Realization of Two-Slit Interference with Atoms

We now turn to the experimental situation to be modeled. We consider the details of the setup of the Shimizu experiment briefly described in Section 1. The particles used in this experiment are $1s_3$ metastable neon atoms with a mass of $m = 3.349 \times 10^{-26}$ kg. A 598 nm laser is used to excite trapped $1s_5$ atoms into the $2p_5$ state, where roughly half will decay to the $1s_3$ state [8]. This state is chosen because of the method by which the atoms are trapped. The atoms are trapped by four laser beams in a magneto-optical trap. The $1s_3$ state is unaffected by the 640 nm lasers creating the trap, thus they are free to fall and their trajectories are determined only by their initial velocities and the acceleration due to gravity [8]. Additionally, this

state is easily detected by a microchannel plate detector which can then be used to display the interference pattern. The size of the cloud of atoms within the trap is roughly 1 mm in diameter [8]. Through an optical fiber in the top of the trap, the 598 nm laser was introduced to excite the atoms. Using cooling lasers, the temperature of the trap was lowered to around 2.5 mK [8]. The initial velocities of the neon atoms follow a Gaussian distribution with an average value of zero and a standard deviation of around 1 m/s, determined by the mass and temperature [8]. The velocity change during the transition of states is negligible. As the $1s_3$ atoms are released, they are funneled into a narrow transfer beam [8]. The resulting atomic source then has a diameter of about 30 μm in the horizontal directions, and roughly 1 mm in the vertical direction [8]. These atoms then fall vertically due to gravity and pass through a double slit placed 76 mm below the trap. The slits have widths of 2 μm and are separated by 6 μm, measured center to center. The atoms then fall a further 113 mm before colliding with the microchannel plate detector. The image produced is then amplified and recorded [8]. Figure 3 provides two schematics of the setup.

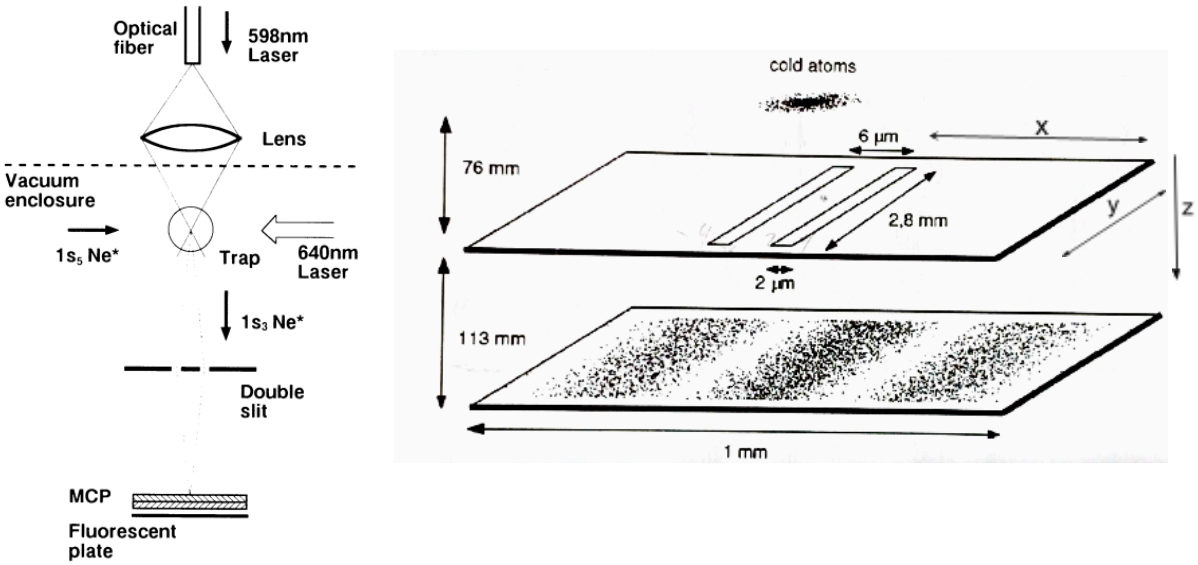

Fig. 3. *Left*: Schematic experimental configuration of the Shimizu experiment highlighting the magneto-optical trap and atomic source from Ref. [8]. *Right*: Schematic configuration of the Shimizu experiment highlighting the slits and dimensions from Ref. [11].

5. The Feynman Path Integral Method applied to the Shimizu Two-Slit Experiment

The Feynman Path Integral Method can now be applied to the Shimizu experiment. Our solution is informed by the treatment in Ref. [11]. The initial distribution of the atoms is described by a three-dimensional Gaussian, with the standard deviation in both the x and y directions given by $\sigma_0 = \sigma_x = \sigma_y = 10\ \mu m$, while $\sigma_z = 0.3\ mm$, reflecting the diameters given in Section 4. Additionally, the initial velocities, described by a Gaussian distribution, can be converted to initial wave numbers, given by $2\pi/\lambda$, with an average of zero and a standard deviation of $\sigma_k = \sigma_{k_x} = \sigma_{k_y} = \sigma_{k_z} \simeq 2 \times 10^8 m^{-1}$. The "k" represents the wave vector defined by:

$$k = mv/\hbar \tag{26}$$

where v is the velocity vector. The dimensions of the slits and the distances in the setup, as displayed in Fig. 3, will be referred to as: $l_1 = 76\ mm$, $l_2 = 113\ mm$, $b = 2\ \mu m$, and $d = 6\ \mu m$.

The initial wave function at time $t = 0$ for an atom described by this setup is given by Equation (27).

$$\Psi_0\left(x, y, z; k_{0x}, k_{0y}, k_{0z}\right) = \Psi_{0_x}\left(x; k_{0x}\right)\Psi_{0_y}\left(y; k_{0y}\right)\Psi_{0_z}\left(z; k_{0z}\right)$$

$$= \left(2\pi\sigma_0^{\,2}\right)^{-1/4} e^{-x^2/4\sigma_0^{\,2}} e^{ik_{0x}x} \times \left(2\pi\sigma_0^{\,2}\right)^{-1/4} e^{-y^2/4\sigma_0^{\,2}} e^{ik_{0y}y} \times \left(2\pi\sigma_z^{\,2}\right)^{-1/4} e^{-z^2/4\sigma_z^{\,2}} e^{ik_{0z}z} \tag{27}$$

In order to propagate this wave function, the kernel is then needed. The process for finding the three dimensional kernel is analogous to the one outlined above. In fact, the three dimensional kernel can be expressed as the product of the kernel in each dimension:

$$K\left(b, t_b; a, t_a\right) = K_x\left(x_b, t_b; x_a, t_a\right)K_y\left(y_b, t_b; y_a, t_a\right)K_z\left(z_b, t_b; z_a, t_a\right) \tag{28}$$

The *x* and *y* kernels are simply the free particle kernel from Eq. (25), with the *x* and *y* positions of the endpoints in the numerator of the exponential, respectively:

$$K_x(b, a) = \left(\frac{m}{2\pi i\hbar(t_b - t_a)}\right)^{1/2} exp\left\{\frac{im(x_b - x_a)^2}{2\hbar(t_b - t_a)}\right\} \tag{29a}$$

$$K_y(b,a) = \left(\frac{m}{2\pi i\hbar(t_b - t_a)}\right)^{1/2} exp\left\{\frac{im(y_b - y_a)^2}{2\hbar(t_b - t_a)}\right\} \quad (29b)$$

The *z* kernel is similar to the free particle kernel, but with a second exponential factor due to the gravitational acceleration in the *z*-direction.

$$K_z(b,a) = \left(\frac{m}{2\pi i\hbar(t_b - t_a)}\right)^{1/2} \times exp\left\{\frac{im(z_b - z_a)^2}{2\hbar(t_b - t_a)}\right\} \times exp\left\{\frac{im}{\hbar}\left(\frac{g(z_b + z_a)(t_b - t_a)}{2} - \frac{g^2(t_b - t_a)^3}{24}\right)\right\} \quad (29c)$$

With the kernel worked out, we can now propagate the wave function according to Eq. (23), with the initial amplitude given by Eq. (27). If we substitute Eqs. (27-29) into Eq. (23) we see that we can separate the variables:

$$\Psi(x, y, z, t; k_{0x}, k_{0y}, k_{0z}) = \int_{(x_a, y_a, z_a)} [K(x, y, z, t; x_a, y_a, z_a, t_a) \times \Psi_0(x_a, y_a, z_a, t_a; k_{0x}, k_{0y}, k_{0z})] dx_a dy_a dz_a$$

$$= \Psi_x(x, t; k_{0x})\Psi_y(y, t; k_{0y})\Psi_z(z, t; k_{0z}) \quad (30)$$

Thus, we can solve each dimension separately:

$$\Psi_x(x, t; k_{0x}) = \int_{x_a} K_x(x, t; x_a, t_a = 0)\Psi_0(x_a; k_{0x}) dx_a \quad (31)$$

The *z*-direction is treated classically as an approximation. Thus, taking into account the effect of gravity, the *z* coordinate of the particle can be written as:

$$z(t) = z_0 + v_{0z}t + gt^2/2 \quad (32)$$

and the arrival time of the particle at the slits is given by t_1.

$$t_1(v_{0z}, z_0) = \sqrt{2(l_1 - z_0)/g + (v_{0z}/g)^2} - v_{0z}/g \quad (33)$$

For a particle starting at z_0=0 at rest, t_1 is roughly 124 ms, and the velocity at the slits, $v_{z1}=gt_1$, is 1.22 m/s. This means that for the neon atoms the de Broglie wavelength, Eq. (3), at the slits is 1.6×10^{-8}m. In this simulation, the distance z after the slits acts as a proxy for the time that has elapsed since the particles traveled through the slits. The particles only exist at a given distance for an instantaneous moment, and do not travel back to that distance at any future

time. Thus, when we describe the probability distribution of the particle at a distance after the slits, we are describing the distribution at a specific time. In this simulation there is not one group of particles at the slits and another group of particles at a different distance at the same time. Our description of the evolution of the distribution as the particles travel away from the slits is a description of the evolution through time.

In the *y*-direction, the slits are very long compared to their other dimensions. For simplicity, we can make the approximation that the slits are infinitely long, and thus there is no spatial constraint on *y*. We can then apply Eq. (31) for the *y*-dimension, using Eqs. (27, 29b) and solve the integral over all possible values of y_a to obtain Ψ_y.

$$\Psi_y\left(y, t; k_{0y}\right) = \left(2\pi {s_0}^2(t)\right)^{-1/4} exp\left\{\frac{-\left(y-v_{0y}t\right)^2}{4\sigma_0 s_0(t)} + ik_{0y}\left(y - v_{0y}t\right)\right\} \quad (34)$$

Here, $s_0(t) = \sigma_0(1 + i\hbar t/2m{\sigma_0}^2)$ and v_{0y} is the initial velocity in the *y*-direction. Now that both the *y* and *z*-directions have been solved, only the *x*-direction remains.

Since the *x*-direction is not solved using either of the approximations of the other two directions, the wave function must be solved in two steps. The first step is the behavior before the particle reaches the slit at time t_1. Before the particle reaches the slit, it is simply moving in free space, with no constraints. Thus, the behavior in the *x*-direction before the slits is the same as the behavior in the *y*-direction, and we can use the result from Eq. (34). Therefore, the behavior in the *x*-direction before the slits is given by Equation (35).

$$\Psi_x\left(x, t; k_{0x}\right) = \left(2\pi {s_0}^2(t)\right)^{-1/4} exp\left\{\frac{-\left(x-v_{0x}t\right)^2}{4\sigma_0 s_0(t)} + ik_{0x}\left(x - v_{0x}t\right)\right\} \quad (35)$$

The dispersion of this wave function means that only a small percentage of the atoms released towards the slits will actually pass through. When the atoms reach the slits at t_1, the probability is a Gaussian distribution whose standard deviation is dependent on $s_0(t_1)$. Since $s_0(t)$ increases with time, this standard deviation is large enough that only 0.1% of the atoms pass through the thin slits.

The second step is then the behavior after the particle passes through the slits at time t_1 up to its impact at the detection plate. The time at which it impacts the plate can be solved for the same way as t_1, Eq. (33), with l_1 being replaced by $l_1 + l_2$. For a particle starting at z_0=0 at rest, t_2 is roughly 196 ms. After the particle has passed through the slits, it is once again traveling in free space with no restraints, so the wave function can be solved in a similar way as before, but the initial amplitude is now only present in the two slits, not a Gaussian distribution. As explained in Section 2, the two slits act as two non-exclusive alternatives, and follow Eqs. (6-8). Thus, we find the total wave function after the slits by adding the amplitudes from each slit, labeled Ψ_A and Ψ_B.

$$\Psi_x\left(x, t; k_{0x}, k_{0z}, z_0\right) = \Psi_A + \Psi_B \tag{36}$$

In Eq. (36) k_{0z} and z_0 are used to determine t_1 via Eqs. (26, 33).

In order to calculate Ψ_A and Ψ_B, we remember that the particle is traveling in free space after the slits, and thus use Eq. (31) with the free space kernel from Eq. (29a). The difference between this calculation and that of Eqs. (33, 34) is that the initial wave function is no longer that of Eq. (27). The particle has traveled to the slits and is thus described by Eq. (35) with $t = t_1$. Additionally, when we apply Eq. (31) we must now integrate only over the values of x_a or x_b that lie within the slit, since the amplitudes that impact the walls around the slits should not be allowed to propagate to the screen. Thus, Ψ_A and Ψ_B are given by:

$$\Psi_A = \int_A K_x\left(x, t; x_a, t_1\left(v_{0z}, z_0\right)\right)\Psi_x\left(x_a, t_1\left(v_{0z}, z_0\right); k_{0x}\right)dx_a \tag{37a}$$

$$\Psi_B = \int_B K_x\left(x, t; x_b, t_1\left(v_{0z}, z_0\right)\right)\Psi_x\left(x_b, t_1\left(v_{0z}, z_0\right); k_{0x}\right)dx_b \tag{37b}$$

The integration over A and B signify integration over the x_a and x_b positions spanning each of the slits. With these, we are able to calculate Ψ_A and Ψ_B at any horizontal location, x, at a time after the particle has passed through the slits. Adding the two amplitudes to obtain the total

amplitude and then taking the absolute square then gives us the probability of the particle to be at that point at that time.

If we repeat this process for every point on the screen at the time that the particle reaches the screen due to its gravitational acceleration, we would then have the probability distribution of the particle at the screen. Thus, we can use this method to find the probability distribution of the particles interacting with the two slits. If we similarly perform this calculation for a range of x positions at an earlier time, we would then have the probability distribution of the particle at a location between the slits and the screen. Thus, using this method with many different times, we can observe how the probability distribution of the particle changes as the particles travel through time.

5.1. Creating the Code

In order to implement this method, we created a Python program to perform the necessary calculations outlined in the previous sections. This program makes use of the NumPy and Matplotlib libraries to perform the calculations and plot the results. Firstly, we set all the necessary constants equal to their physical values, as described in the Shimizu experiment. We then define the kernel in the x-direction as a function, using Eq. (29a). This function takes as inputs the initial and final x-positions and times, calculates the coefficient and exponent, and returns the kernel as defined in Eq. (29a). The result is the kernel for propagation through free space between two specified points at two specified times.

In order to create the wave function before the slits, Eq. (35), we then represent $s_0(t)$ as a function with time as its argument. With that we are able to define the function to represent Ψ_x before the slits, as a function of x, t, and k_{0x}. This function first calculates the velocity of the particles from the wave number via Eq. (26). Then the function builds up Ψ_x by calculating the coefficient and the real and imaginary parts of the exponent, according to Eq. (35), using the function for $s_0(t)$ just defined and the value for v_{0x} just calculated before. The function then

returns the wave function of the particle before the slits at a single location and time specified by the inputs.

In order to convert the distance after the slits to the time the particle has been traveling, we create a function to implement Eq. (33). This function takes in the distance after the slits and returns t_1, the time it takes for the particle to reach the slits based on l_1, and t, the time it takes the particle to travel the specified distance after the slits.

The next step is to perform the integral for a single slit from Eq. (37). We define a function to solve this integral, taking in as parameters: a list of horizontal x-locations where we want to solve for the amplitude after the slits, the locations of the edges of the slit, the distance from the slits we are calculating at, and k_{0x}. The first step is to convert the distance from the slits to time, using the function described above, giving us t_1 and t. We then use the locations of the edges of the slit to create an array of 2000 evenly spaced points spanning the slit. We then use a "for loop" to perform the integral from Eq. (37), looping over the slit points and using a Riemann sum to approximate the integral. Within the loop, we calculate the amplitude from Eqs. (37a,b)

$$K_x\left(x, t; x_a, t_1\left(v_{0z}, z_0\right)\right)\Psi_x\left(x_a, t_1\left(v_{0z}, z_0\right); k_{0x}\right)$$

using t and t_1 as above, and the slit point as x_a. The free particle kernel and Ψ_x are given by the previously defined functions, taking the appropriate parameters. This amplitude is then added to a total amplitude for the loop. Once we have looped over all of the slit points, the total amplitude is then the sum of the amplitudes from each slit point. This total is then multiplied by the distance between each slit point. Thus, we approximate the integral of Eq. (37) with a Riemann sum over 2000 points spanning the slit.

The result of that integral approximation is Ψ_A at the point x at time t. This amplitude is then saved to a list of amplitudes. The entire process is then repeated for each x-location that we want to solve for by using a second "for loop" over the list of x-locations. Each resulting Ψ_A

from this loop is saved to the list of amplitudes. This function then returns this list, giving us the Ψ_A amplitudes from Eq. (37) for a range of locations along the screen.

We then create a two-slit probability function, which takes all the same inputs as the one slit amplitude function, with extra parameters to describe the edges of both slits. This function takes the parameters and the edges of the first slit, and uses the one slit amplitude function above to calculate the amplitude along the range of *x*-locations from the first slit. We then repeat this process for the second slit, using the appropriate slit edges. Once the one slit amplitude has been done twice, once for each slit, we then add the two lists of amplitudes pointwise to obtain the total two-slit amplitude at each point, following Eq. (36). We then take the absolute square of each element in this list, following Eq. (6), to obtain a list of the probabilities at each point. Thus, we now have a list of the probabilities along a range of *x*-locations for particles traveling through the two-slit experiment at a distance we choose. Using this code at different distances from the slits, we can observe the evolution of the probability distribution for particles passing through the two slits.

6. Visualization

To visualize this evolution we can use two different methods. The first method is a two dimensional plot in the *x* and *z* directions, with color representing the probability of the particle to be at that point. We can make this by creating a function with the same parameters as the two-slit probability function, with the distance from the slits replaced by a list of distances spanning the desired range. The first step in this function is to create a matrix with the number of rows equal to the number of distances from the slit in the *z* direction and the number of columns equal to the number of *x*-locations we are calculating for. Then, for each distance in the list, we apply the two-slit probability function at that distance. We then set the corresponding row of the matrix equal to the resulting list of probabilities. We do this for each distance in the list, setting successive rows equal to the probability list at successive distances. Finally, to visualize

the data contained in the matrix, we use Matplotlib's Pyplot.Imshow function to plot the matrix as a grid of squares, with the color of each square corresponding to the matrix entry's value. In the color mapping that we use, higher probabilities are red, lower probabilities are blue, and values in between follow the order of the rainbow. We then can add the appropriate axes to the plots. An example of this type of visualization is shown in Figure 4.

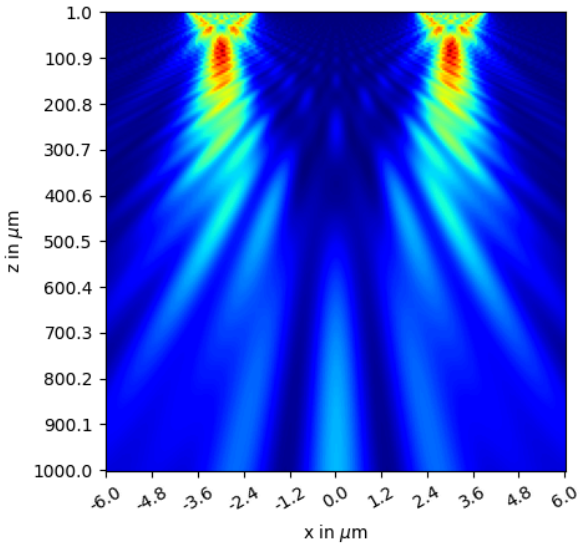

Fig. 4. Example of the matrix visualization of the evolution of the probability. Shown here for neon atoms for the first millimeter after the slits.

The second method to visualize the evolution is to create a series of line plots along the *x*-direction at different distances, with the line's height representing the probability at that point. We can again make a function to make these plots. At each distance we can use the two-slit probability function to obtain the list of probabilities over a range of points. We can then plot this list along the y-axis, and the points in the range on the x-axis using Matplotlib's built-in plotting functions. We can then input different distances into the two-slit probability function to create the series of plots to see the evolution of the probability. An example is shown in Figure 5.

With our two methods, we can visualize the evolution of the probability of the particles traveling through the two slits through the near and far regions. In the further Fraunhofer region we can compare our probability distribution to the Fraunhofer distribution of the optical two-slit

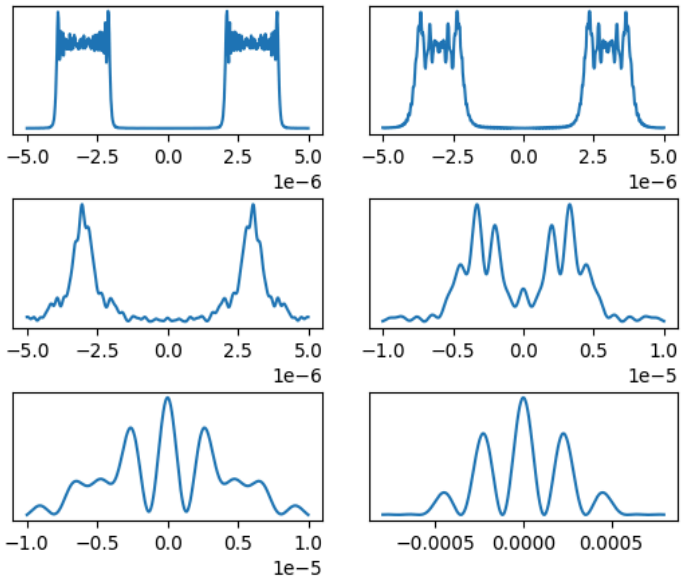

Fig. 5. Example of the line plots visualization of the evolution of the probability. Shown here for neon atoms for various distances after the slits.

problem. As in Section 1, the Fraunhofer double-slit diffraction gives an equation for the irradiance of light traveling through the slits at a point on the screen far away, Eq. (1a). Since the optical two-slit problem treats light in the same way we are treating the probability, we can apply this equation to obtain the Fraunhofer estimation of our probability distribution to cross check our calculations in the far region. We can create functions in our code for each of Eqs. (1a-c) that together return the estimated irradiance at a point on a screen at a specified distance from the slits. We then apply this function to a list of points in the *x* direction and plot the resulting irradiances against their locations. We can then compare this plot to our previous plots of the probability at that distance. Comparing these plots at different distances allows us to cross check our solutions within the Fraunhofer region and allows us to observe the differences between the probability and the Fraunhofer approximation at closer distances. An example of one of these checks within the Fraunhofer region is given in Figure 6. We can use Eq. (2) to find the boundary for this region. For the Shimizu experiment, *a* is 6 μm, but the velocity of the atoms is increasing over time. To estimate the de Broglie wavelength, Eq. (3), we take the

midpoint between the velocity of the atoms at the slits and their velocity at the screen, which comes to $v = 1.57\, m/s$. With the associated de Broglie wavelength of 1.26×10^{-8} m, Eq. (2) gives the boundary of the Fraunhofer region at around 3 mm. We plot the comparison between the distributions at a distance of 113 mm, substantially larger than the boundary. In Eq. (1a), the irradiance is given by a proportionality, rather than an exact equation. In order to compare the distribution to the Fraunhofer approximation, we scale the approximation so that its maximum value is equal to the maximum value of the probability distribution. Thus, the highest peaks of each are set to the same height. We see in Fig. 6 that after this scaling, the rest of the peaks continue to agree. We can see that our probability distribution matches the Fraunhofer distribution in this region.

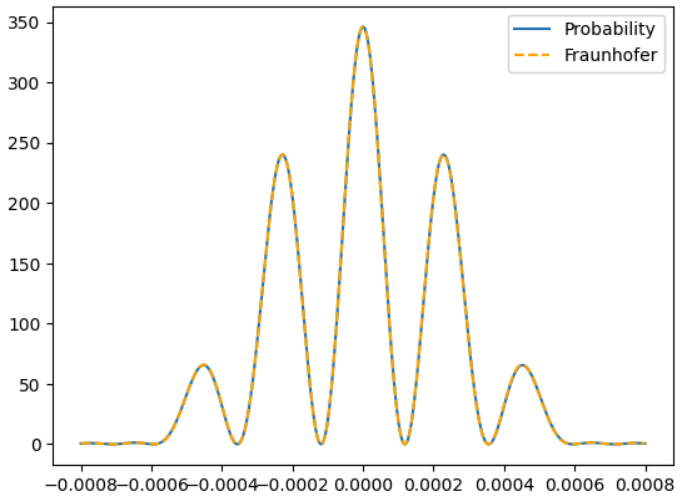

Fig. 6. Example comparison of the Fraunhofer approximation to our calculated probability distribution at 113 mm, a distance greater than the 3 mm boundary of the Fraunhofer region.

7. Results of the Toolkit

We now present the results of our toolkit through the visualizations it has produced and compare them to theoretical expectations and the results of previous works. First, we present the results of our simulations of the Shimizu experiment and the behavior of the neon atoms subjected to the two-slit experiment under the effects of gravity. We also compare these

visualizations to those produced by Ref [11]. Figure 7 displays the two-dimensional color plot of the evolution of the probability distribution from the source to the screen from our toolkit compared to the similar plot from Ref [11].

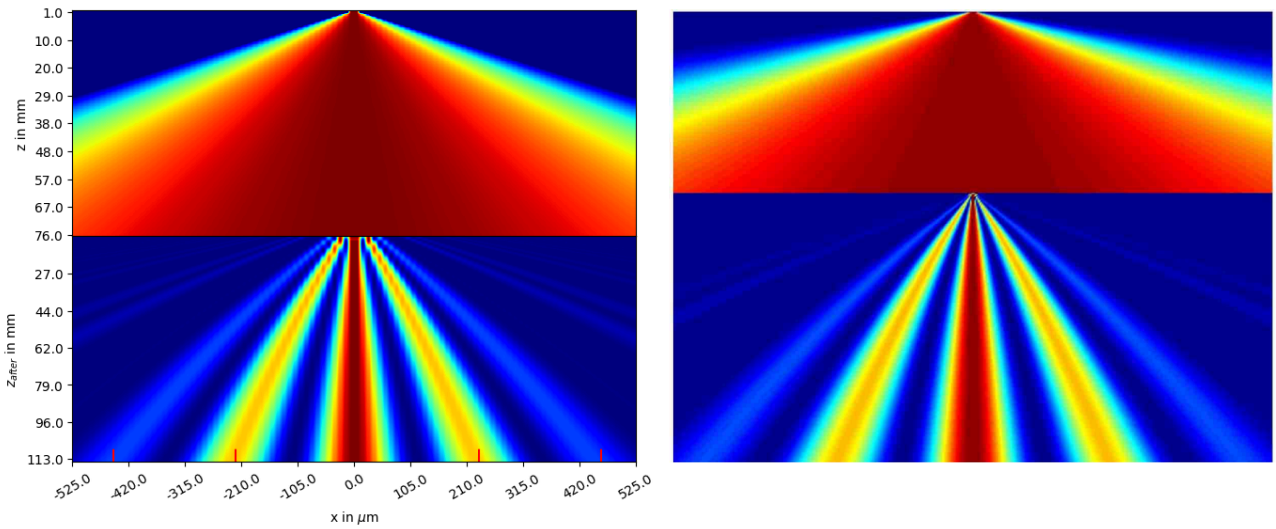

Fig. 7. *Left*: Two-dimensional color plot of the evolution of the probability distribution from the source to the screen. The two slits lie in the middle of the figure. The top half is the distribution before the slits, and the bottom is after. Small red lines at the bottom of the figure signify the fringe locations from the Shimizu experiment. *Right*: Evolution of the probability density from the source to the detector screen from Ref [11]

In Fig. 7 the two slits lie in the middle of the left plot, at the $z = 76\,mm$ mark. The slits are slightly higher in the right plot, at the location where the behavior abruptly changes. In the horizontal direction, the slits lie between -4 μm and 4 μm, taking up only 0.76% of the horizontal axis. The top portions of the two plots represent the distribution of the atoms before they interact with the slits, and the bottom portion is after they pass through the slits. We can see in these plots how the wave function before the slits spreads as a Gaussian as time increases, as mentioned in Section 5. Once the atoms reach the slits, the distribution is easily spanning the horizontal axis. When compared to the small portion of the axis that the slits cover, the dispersion is enough that only a small percentage of the atoms pass through the slits, and the rest are blocked. In the behavior after the slits, at this scale, we can immediately see the

large-scale interference between the two slits. The spacing between the bright fringes is consistent at any given time, and grows as time increases. The two plots shown in Fig. 7 display the same behavior for the neon atoms as they travel to the screen. Our implementation of the path integral method visually agrees with the figure from Ref [11]. The small red lines on the horizontal axis of the left plot are placed at the locations of the fringes observed on the screen in the Shimizu experiment. The spacing they observed was roughly 227 μm [8], and the four lines are placed at the integer multiples of this spacing. We can see that the spacing observed by Shimizu agrees with our simulation of the experiment.

The behavior depicted in Fig. 7 resembles the behavior of the Fraunhofer approximation, depicted in Fig. 1, with its equal spacing of fringes whose maxima decrease as they move away from the middle. This behavior is expected at the screen since it is far from the slits. In order to observe the behavior in the geometric and Fresnel regions, we must focus our visualizations closer to the slits. Figure 8 displays the same comparison of the probability evolution for the first millimeter after the slits.

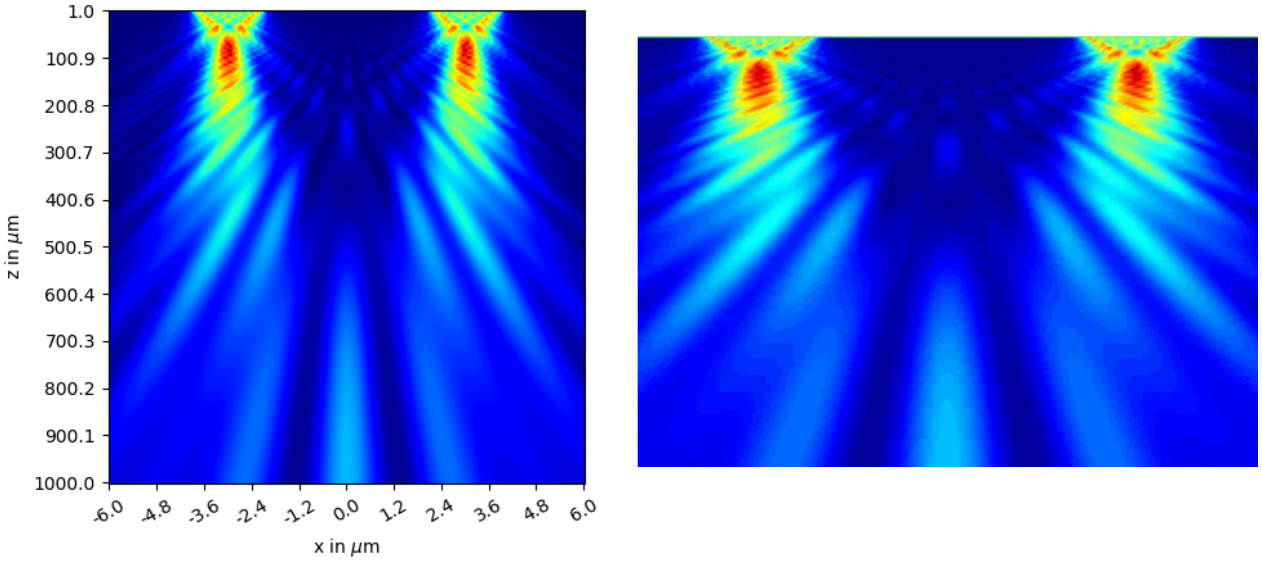

Fig. 8. *Left*: Two-dimensional color plot of the evolution of the probability distribution for the first millimeter after the slits. *Right*: The respective plot from Ref [11].

For the first millimeter after the slits, the two visualizations again appear nearly identical, outside of differences in scaling. In the first millimeter we see that very close to the slits, the distribution appears as nearly an image of the slits as expected in the range of geometric optics. As the atoms continue to fall, the distribution begins to display the growth of the fringed edges of the Fresnel region. Within this first millimeter we also observe the beginning of the interference between the waves from the two slits. Immediately after the slits, their contributions are separate, but by the bottom of the plots they are interfering and overlapping with each other. Very near the slits, when the contributions are separate, we also see the diffraction pattern caused by each individual slit, without any interference between them. By the time the atoms reach 1 mm from the slits, they have not yet formed the Fraunhofer fringe pattern of Fig. 7. The behavior seen in Fig. 8 is the behavior of the Fresnel region and is a demonstration of the complex behavior observed outside of the Fraunhofer approximation.

We next focus even closer to the slits, simulating only the first 100 μm after the atoms pass through the slits. The visualizations at this distance are presented in Figure 9. In the first 100 μm the interference effect is not yet apparent between the two slits. This un-interfering distribution would not be obtainable if we had only simulated the experiment with the Fraunhofer estimation. We can also more clearly see the sharp image of the slits right after the atoms pass through, while they are still near the regime of geometric optics. As the particles travel the 100 μm however, we see how the faint fringes begin to emerge from the background, as expected of the Fresnel region. We again see the diffraction patterns caused by the individual slits, before they interfere. This area, within the first 20 μm or so, is an interesting location for future study. Further simulations could investigate and describe these individual diffraction patterns and further analyze the behavior close to the slits. With these three sets of plots we observe how the probability distribution evolves through and across the three regions. We are also able to observe the fine structures that exist before the Fraunhofer distribution arises.

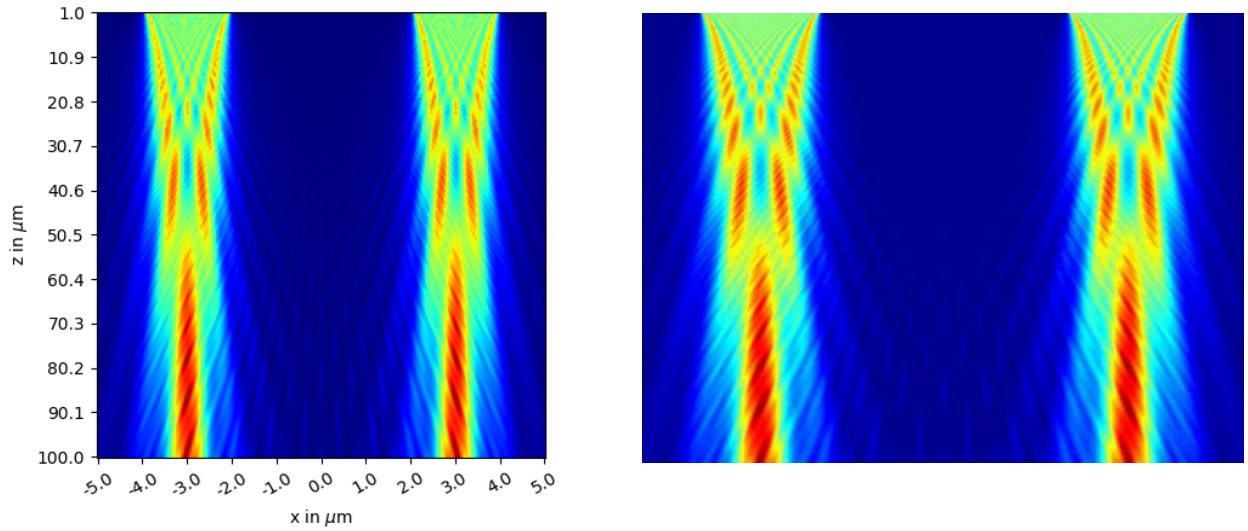

Fig. 9. *Left*: Two-dimensional color plot of the evolution of the probability distribution for the first 100 μm after the slits. *Right*: The respective plot from Ref [11].

While the two-dimensional color plots allow us to easily observe the continuous growth and evolution of the probability distribution over time, we can use our line plot function to more quantitatively observe the distribution and compare our results. In Figure 10 we create a series of line plots at different distances where the height represents the probability of the atom to be at that point, and compare those results to those of Ref [11].

In the plots from Ref [11] there is a second set of dotted lines on each plot that represents the sum of the probability distributions from the slits separately. While these lines do demonstrate that the overall probability distribution is not the sum of the individual probabilities, rather we must use Eqs. (6-8), we will compare our plots to the solid lines. When we compare the results of our toolkit to these plots, we see that they show the same behavior in each plot. This agreement is easier to see in Fig. 10 than in Figs. 7-9. This method of visualization allows us to better understand the distribution at a given distance, while the series of plots still allows us to visualize the evolution over time. Additionally, with these plots we can more easily see the different regions discussed in Section 1. In the first two plots, the distribution is a sharp image of the slits, as we expected. As we travel further from the slits in the next two plots, the images of

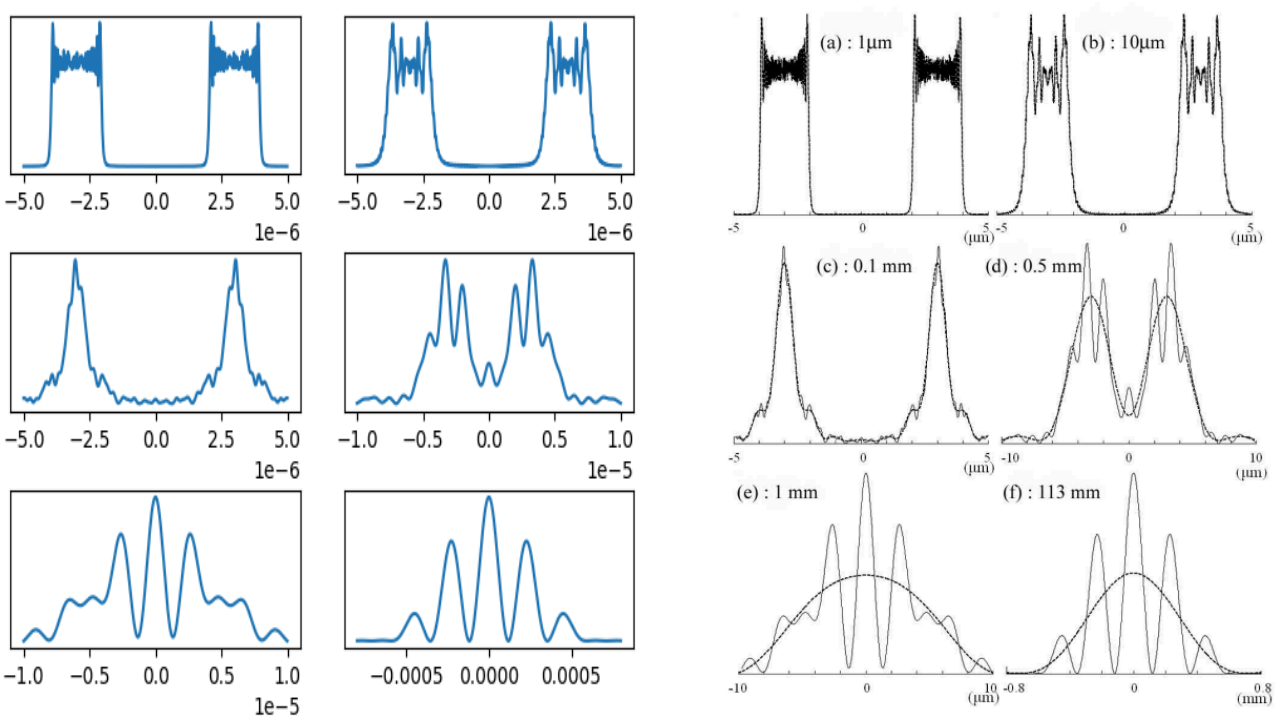

Fig. 10. *Left*: Series of line plots whose height represents the probability of the atoms to be at that point. The x-axis represents the *x*-dimension in the Shimizu experiment. The powers beneath the first five x-axes are the scales for those plots, specifically, micrometers or tens of micrometers. The plots are created at 6 distances from the slits: 1 μm, 10 μm, 0.1 mm, 0.5 mm, 1 mm, 113 mm. *Right*: The corresponding plot from Ref [11]. The solid line is the probability we are comparing to; the dotted line is the sum of the probabilities from each slit to show that it does not give the same distribution as summing the amplitudes and then squaring.

the slits gain fringes on the edges and become more pointed than square. We also begin to see the interference of the two slits around the 0.5 mm point, as in Fig. 8. Finally, the last two plots display the progression towards Fraunhofer behavior. As we travel further from the slits, the plots become more like the Fraunhofer distribution from Fig. 1.

Through these four sets of plots we have demonstrated that our simulated behavior agrees with the description of the behavior resulting from the two-slit experiment, in all three regions. The behavior of the neon atoms subjected to the two slit experiment by Shimizu is the same behavior as that of light subjected to the same setup. This agrees with de Broglie's assertion that particles also act like waves. We also have shown that our program agrees with

the method from Ref. [11] on which we have based it. Now that we have successfully followed this method and created a framework which agrees with it, we can expand our toolkit to investigate other experiments.

8. Generalization of the Code

We next expand our program to allow for more experimental setups to be investigated. This generalization will expand our program from a numerical simulation of the Shimizu experiment to an adjustable toolkit that can be used to explore many existing experiments and can be used to create theoretical expectations for new experiments. In order to expand our program, we first allow changes to be made to the particle subjected to the two-slit experiment. The mass of the particle is an important value that is used in many of the equations that our code solves. Each function we have defined uses the mass of the particle. For ease, the mass of the particle is stored as a variable at the beginning of the program, and this variable is called whenever one of the functions needs the mass. This means that changing the value of the variable will change the mass of the particle in every equation. Thus, only one line needs to be changed to investigate different particles. Instead of investigating the behavior of the neon atoms from the Shimizu experiment, the mass variable could easily be changed to the mass of the electron. Therefore, this toolkit could be used to calculate the behavior of electrons or other particles, expanding its applications.

Similarly to the particle mass, the size of the initial wave function is also defined by a variable. In Eq. (35) we give the wave function in the *x*-direction before the slits and the value of this calculation at different locations is used to find the behavior after the slits. In Eq. (35), we start with a Gaussian wave function at time $t = 0$, which we then see expand based on the initial standard deviation and time that has passed. This initial standard deviation is given by σ_0, which is defined by a variable in our code. Similarly to the mass, this variable is called whenever σ_0 is needed, as in the $s_0(t)$ function, meaning that we can just change the variable in order to

change the entire setup. We can then describe the initial distribution of the particles by a Gaussian of any size, expanding the range of experiments that could be simulated. Additionally, we could, although not done in this paper, make the initial wave function a distribution other than a Gaussian. In the program, the Ψ_x function is called within the loop over the slit points in the one slit amplitude function. Since Ψ_x is called as a function, its definition could be changed to reflect some non-Gaussian initial distribution. This type of change would require new code to be written, rather than simply changing the value of a variable, but we would not be required to create a new toolkit for the new distribution. The application of the Feynman Path Integral Method would continue to work, allowing for this toolkit to be applied to even more experimental setups and produce expectations for the behavior of the particles, without a requirement of a Gaussian distribution.

The width and separation of the slits, as well as the distance between the particles' starting point and the slits, are also given by variables that can be easily changed. The distance between the slits and the point of observation is the distance that we are already able to choose and vary to see the evolution of the particle behavior. Thus, all of these dimensions of the setup are customizable as well. While our toolkit focusses on a simulation with two slits, the code could also be adapted to more slits. Our two slit probability function simply performs the one slit amplitude function twice and then sums the resulting amplitudes. Following Eq. (7), the more amplitudes could be added to this sum. Thus, a new function could be created that performs the one slit amplitude function for three or more slits, and then sums the results before taking the absolute square. While this setup is not currently a part of the toolkit, it could be expanded to allow for these experiments, and create simulations and expectations.

The final customization available in the expanded toolkit is the choice between gravitational acceleration of the particles and a constant velocity. In our initial framework we worked to simulate the Shimizu experiment in which the neon atoms fall by the acceleration due to gravity. We created a function to implement Eq. (33) to convert the distance after the slits to

the time that the particle has been traveling. This function took as parameters the distance to the slits l_1 and a distance after the slits, and returned t_1 and t, using the acceleration due to gravity. In order to obtain t_1 and t from a constant velocity, we must create a new function, replacing the implementation of Eq. (33). The new equations to be used are given by Equations (38a,b).

$$t_1 = \frac{l_1 - z_0}{v} \tag{38a}$$

$$t = \frac{z_{after}}{v} + t_1 \tag{38b}$$

In Eqs. (38a,b), v is the constant velocity of the particle and z_{after} is the distance that the particle travels after it has passed through the slits. We can create a function within our toolkit to implement this new method, taking v and z_{after} as parameters and returning t_1 and t. We then create a variable called *grav* that has either the value *True* or *False*. This variable can then be called in all of our functions. When *grav* is True, our program calls the function implementing Eq. (33), and when it is False, it calls the function implementing Eqs. (38a,b). When *grav* is False, we also then call the new velocity variable *v,* whose value is chosen by the user. Whichever method is chosen, the rest of the program runs the same way as before. This new constant velocity function allows for a greater range of experiments to be studied. It also allows us to better compare our results to the Fraunhofer distribution. The Fraunhofer distribution, given by Eqs (1a-c) depends on the wavelength, which for particles is given by Eq. (3). This wavelength is dependent on the velocity of the particles, and thus changes as the particle accelerates due to gravity. The constant velocity function leads to a constant wavelength, allowing us to better compare our distribution to the Fraunhofer approximation. These generalizations to the toolkit allow it to be customized to the needs of experiments beyond the Shimizu experiment, and provide more simulations and expectations to inform the implementation of new experiments.

8.1. Constant Velocity

The first change that we will visualize is the use of a constant velocity instead of gravitational acceleration. This change allows the toolkit to be used for many experiments where the particles are not falling due to gravity, and are propelled in some other fashion. We will compare the distributions of the neon particles in the Shimizu experiment accelerated by gravity, to a simulation of the same atoms with a constant velocity as they travel through the setup. The velocity of the neon atoms will be $v = 1.57\, m/s$. This value is the midpoint between the velocity at the slits and the velocity at the screen when the atoms are being accelerated by gravity. The comparison of the two simulations is shown in Figure 11. The distributions from the constant velocity are very similar to those from the gravitational acceleration. Only the fourth and fifth plots have significant visual differences. The differences arise from the particles having traveled for different amounts of time to get to the same distance from the slits. We can see from Fig. 11 that the atoms with constant velocity have very similar behaviors to the gravitational ones; they go through the same three regions, in a similar amount of time.

Now that we have shown that particles with a constant velocity have the expected behavior in our simulations, we can use them to compare our distributions to the Fraunhofer approximation. For our comparison of the results of our toolkit to the Fraunhofer approximation, we will use particles of constant velocity, since the approximation, Eq. (1a-c), depends on velocity of the particles, via their wavelengths. We will again use neon atoms with a velocity of $v = 1.57\, m/s$. We will use the functions created at the end of Section 6 to produce the Fraunhofer approximations with the wavelength given by the de Broglie wavelength. With this wavelength and the slit separation of 6 μm, Eq. (2) gives that the Fraunhofer approximation is valid at distances much larger than 2.86 mm. The comparisons of our constant velocity distributions and the Fraunhofer approximations at six distances between the slits and the screen are presented in Figure 12. In order to compare the distribution to the Fraunhofer

approximation, we again scale the approximation so that its maximum value equals the maximum value of the probability distribution.

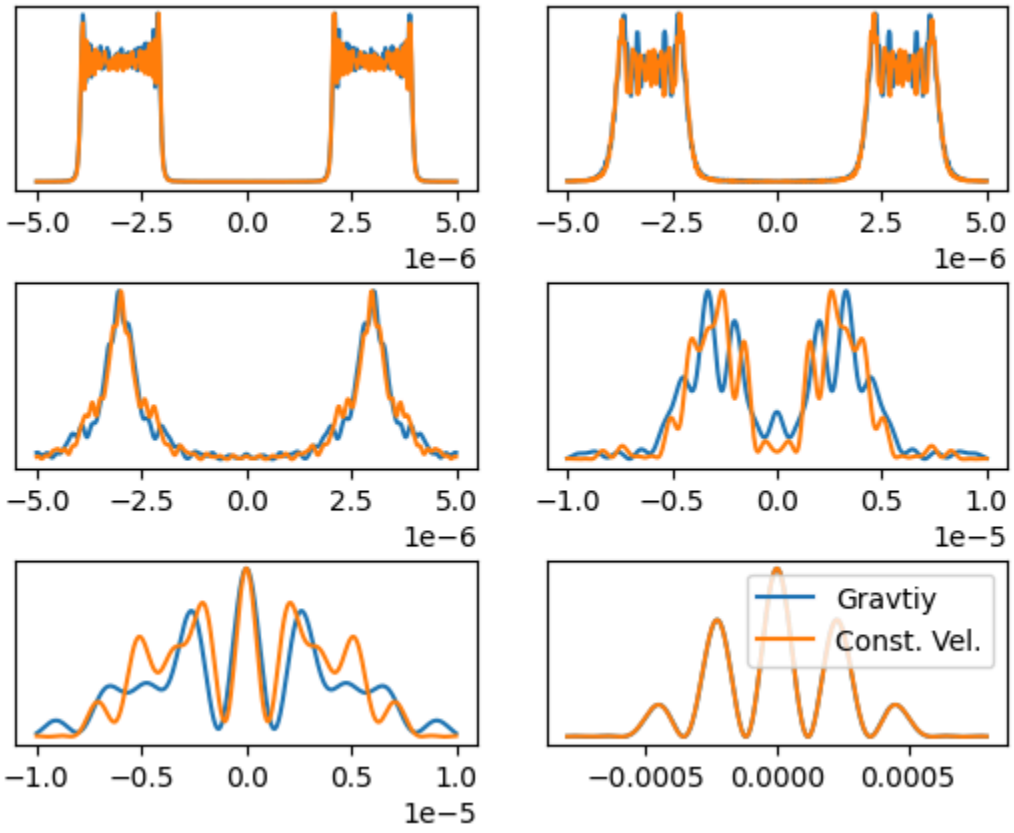

Fig. 11. Series of line plots representing the probability of the atoms to be at a series of points. The plots are created at 6 distances from the slits: 1 μm, 10 μm, 0.1 mm, 0.5 mm, 1 mm, 113 mm. Blue lines represent distribution with acceleration due to gravity. Orange lines represent distribution with constant velocity. The powers beneath the first five x-axes are the scales for those plots, specifically, micrometers or tens of micrometers.

As seen in Fig. 12, the Fraunhofer approximation does not match the probability distribution at all when we are very close to the slits. As the distance from the slits is increased, however, the approximation begins to improve. Once we are very far from the slits, much further than 2.86 mm, the Fraunhofer approximation almost perfectly matches the distribution. The Fraunhofer distribution in this example does not begin to look like the probability distribution until we are roughly 1 mm from the slits, at which point only the three middle fringes are similar. At this point we are close to the boundary of the Fraunhofer region, but are not yet in it. At 3 mm,

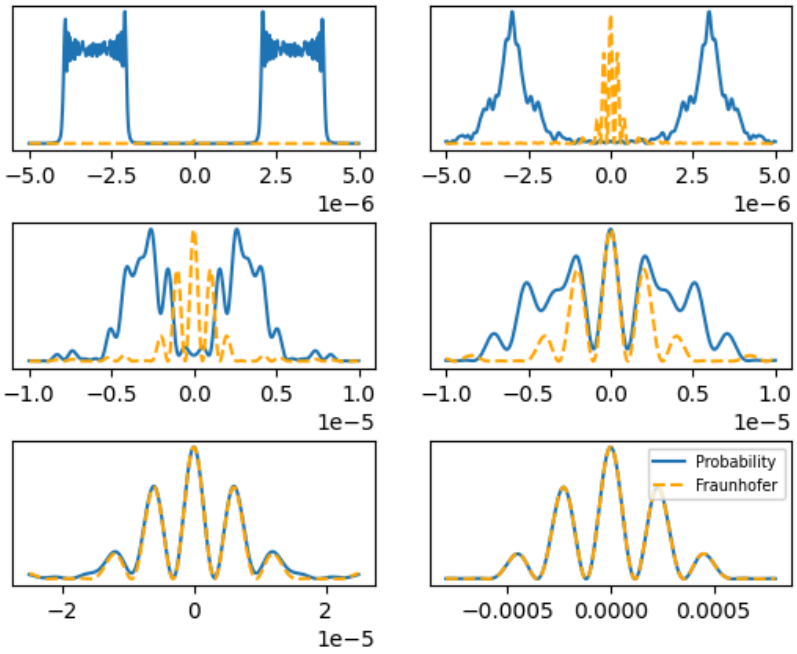

Fig. 12. Series of line plots representing the probability distribution and Fraunhofer approximation at 6 distances from the slits: 1 μm, 0.1 mm, 0.5 mm, 1 mm, 3 mm, 113 mm. Blue lines represent the probability distribution. Orange lines represent the Fraunhofer approximation. The powers beneath the first five x-axes are the scales for those plots, specifically, micrometers or tens of micrometers.

we are barely over the boundary into the Fraunhofer region. Here we see that the two probabilities agree more, but are still not yet perfectly aligned, as seen at around 20 μm horizontally. Once we are at the screen, 113 mm from the slits, the Fraunhofer approximation perfectly aligns with the distribution. Firstly, this comparison gives further legitimacy to the results of our toolkit, since we expect the approximation to be good when we are sufficiently far from the slits. Secondly, we have also now visualized the limitations and the range of the approximation. We are able to observe when the approximation is good enough to be useful. Once we have entered the regime where it is useful, we can more easily and quickly use the approximation, rather than performing the numerous calculations required for our method. This knowledge of when the approximation is useful or applicable can be a valuable resource for the design and investigation of future experiments as it can limit the amount of extra work that

needs to be done. It also provides us with insight into where the less investigated regions of the experiment lie, guiding us towards new information beyond the simple approximation.

8.2. Electrons

The final change to the experiment that we will visualize is the use of electrons as the particles in the experiment, instead of neon atoms. To do this, the mass of the particle in the toolkit is changed to the mass of the electron, $m = 9.109 \times 10^{-31}$ kg. In order to further test the toolkit and to further investigate a new experiment, the other parameters and dimensions were also changed. The distance to the slit from the source of the electrons was changed from 76 millimeters to 1 meter. The widths of the slits were changed to be 0.095 μm, or 95 nm, and the separation between their centers was changed to 335 nm. Additionally, we used a constant velocity of $v = 1.497 \times 10^{8}\, m/s$, or roughly 50% the speed of light, giving a de Broglie wavelength of 4.86 pm. The two-dimensional color visualizations of the behavior in the first millimeter and centimeter are presented in Figures 13 and 14, respectively.

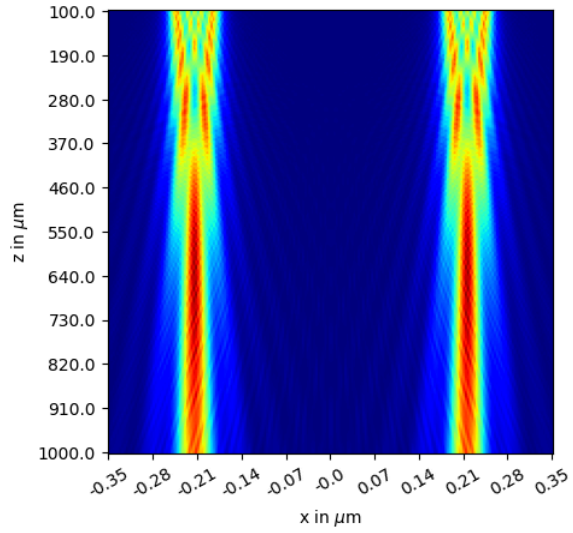

Fig. 13. Two-dimensional color plot of the evolution of the probability distribution of the electron for the first millimeter after the slits.

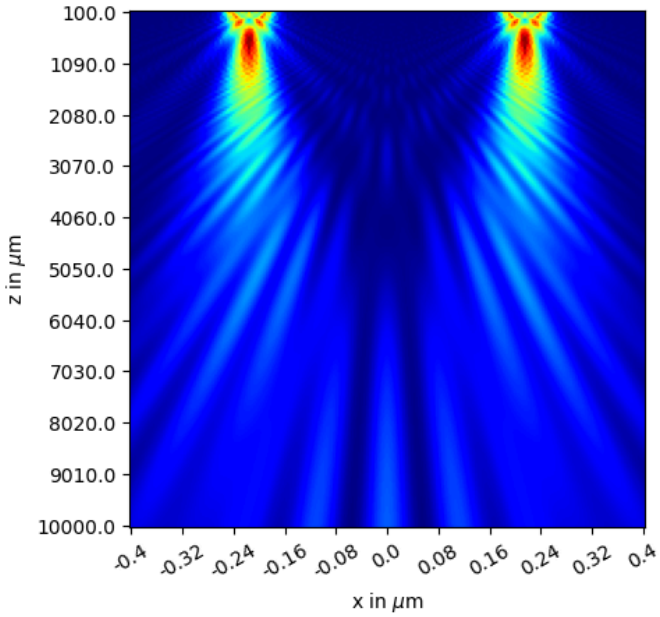

Fig. 14. Two-dimensional color plot of the evolution of the probability distribution of the electron for the first centimeter after the slits.

With all of the changes to the experimental setup, the simulations for the electrons continue to produce visualizations similar to those in Figs. 8 and 9, supporting the robustness of our toolkit. The behavior of the electrons appears the same as that of the neon atoms, but on a different scale. Further simulations and experiments could investigate the nature of this scaling and work towards further describing the behavior close to the slits. We observe the image of the slits at small distances, and this image begins to gain fringes on the edges as we get into the Fresnel region. We also observe how once again the two slits do not interfere with each other initially, and begin to interfere after some distance. The structure of the distributions is the same as described before and agrees with the expectations from the two-slit experiment, simply on a different scale. We present the visualization of the distribution at a further distance of 1 meter from the slit in Figure 15, and a series of line plots of the behavior in Figure 16. We once again see the behavior of the electrons reflecting the behavior of the neon atoms. In Fig. 16 we can again see the evolution of the distribution through the three regions discussed in Section 1.

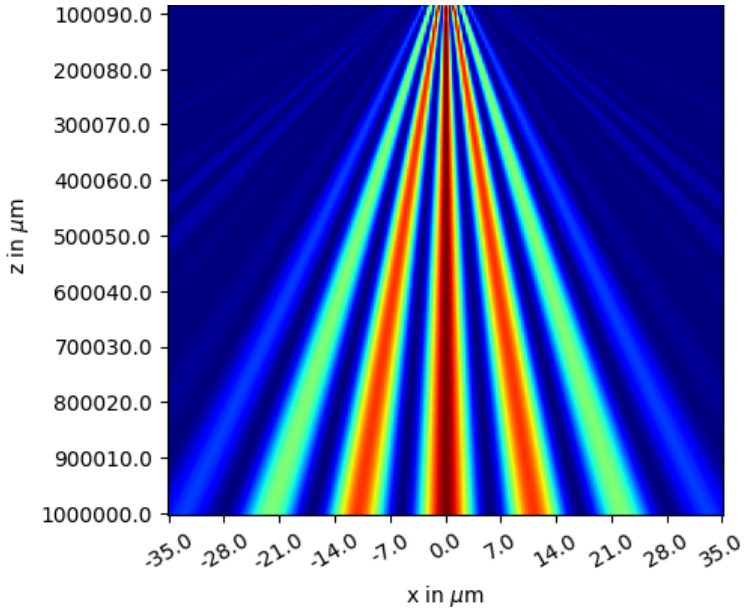

Fig. 15. Two-dimensional color plot of the evolution of the probability distribution of the electron for the first meter after the slits.

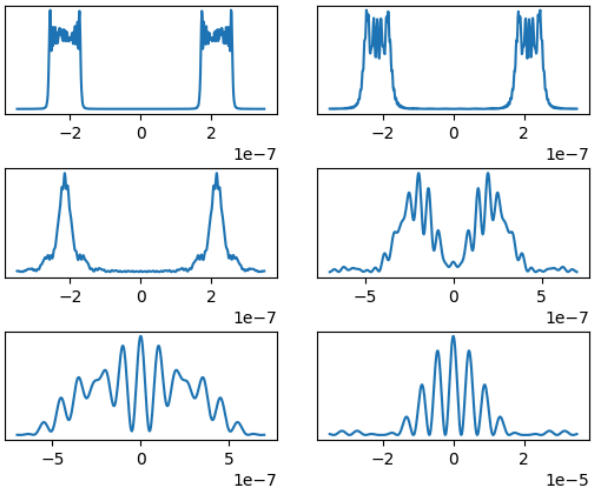

Fig. 16. Series of line plots representing the probability of the electrons to be at that point. The plots are created at 6 distances from the slits: 10 μm, 0.1 mm, 0.8 mm, 5 mm, 9 mm, 0.4 m.

With these two visualizations, we also see that far enough away from the slits, the electrons form a pattern similar to the Fraunhofer distribution. We visualize the comparison between the probability distributions and the Fraunhofer approximation in Figure 17.

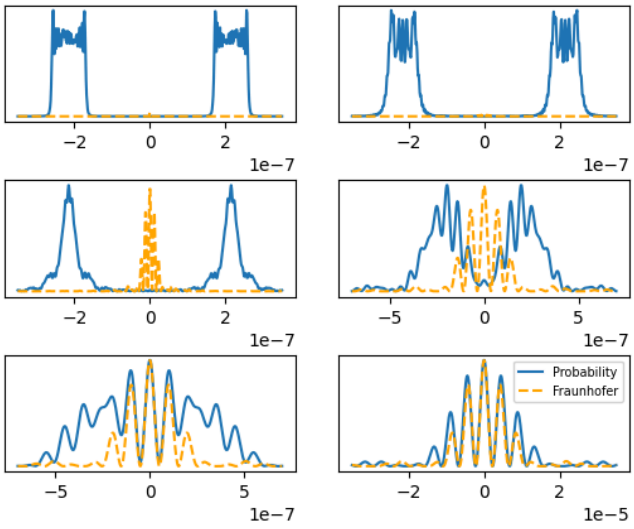

Fig. 17. Series of line plots representing the probability distribution and Fraunhofer approximation at 6 distances from the slits: 10 μm, 0.1 mm, 0.8 mm, 5 mm, 9 mm, 0.4 m. Blue lines represent the probability distribution. Orange lines represent the Fraunhofer approximation. The powers beneath each of the x-axes are the scales for those plots, specifically, tenths of micrometers or tens of micrometers.

With the mass and velocity specified above, Eq. (3) gives the de Broglie wavelength of the electrons to be $\lambda = 4.85 \times 10^{-12}$m. With this wavelength and the slit spacing of 335 nm, Eq. (2) gives that the boundary of the Fraunhofer region lies at 2.3 cm for these electrons. We can see in Fig. 17 that the probability distribution agrees with the Fraunhofer approximation at distances larger than this 2.3 cm, as it did for the neon atoms in their Fraunhofer region. Near the region we begin to see the two agree, but not perfectly, as expected from the behavior of the neon atoms. Again this allows us to view the limitations and range of the approximation. We continue to observe similar behavior as the neon atoms, but on a different scale. Our results also support the robustness of our toolkit. We were able to use our toolkit to investigate an experiment with many differences from the Shimizu experiment, and the results still agreed with theory. This supports our use of this program in new experiments with different setups to investigate the behavior of the probability distribution, both inside and outside the regime of the Fraunhofer approximation. We have observed how the structure of the distribution evolves from

a simple image of the slits, into fringes around the slit images, to complex and interfering patterns, and finally to a simple distribution described by Eqs (1a-c). We have seen this behavior both in the Shimizu experiment the program was based on and in other experiments because of our generalization.

9. Conclusions

The goal of this work was to establish a numerical toolkit that can be used to investigate the two-slit interference pattern outside the Fraunhofer region and can be used to explore future experimental treatments and setups. We created this Python based toolkit by following the methods of Ref [11] to apply the Feynman Path Integral Method to the Shimizu experiment. We then generalized this framework to explore more experiments, allowing for different particles, slits, and a choice of constant velocity instead of gravitational acceleration. We applied this program to electrons and demonstrated that it gave the expected behavior as compared to Ref [11], as well as agreeing with the Fraunhofer approximations, when applicable. This toolkit is available to use and can be found in the appendix. It can then be used to implement the Feynman Path Integral Method to simulate a variety of particles and initial conditions and their subsequent behaviors with different gratings in both the near and far regions. It can be customized to simulate new two-slit experiments and investigate the resulting behavior. These results have been shown to agree with theory including the Fraunhofer approximation, and can be used as theoretical expectations for future experiments to be carried out. Beyond its use of creating theoretical expectations, this toolkit provides both visual and quantitative descriptions of the behavior of the particles in the more complex region of the two-slit experiment. This region is not described by a simple approximation and is often left less explained in quantum mechanics and optics classes than the Fraunhofer region. This program can be used to better understand and explain the closer regions of the two-slit problem and explore the evolution of the probability distribution as the particles travel through it.

Appendix

The customizable toolkit can be found and accessed through github at the link in Ref [16]. The name of the toolkit is “Path_Integral_Two-Slit_Toolkit”. To use the code, the desired parameters and variables can be defined at the beginning by replacing the values currently in place. These include the mass of the particle, the positions and widths of the slits, the distances to the slits and screen, and the standard deviation of the initial Gaussian wave function. Then, by setting the variable *grav* to either *True* or *False*, the particles can be made to accelerate by gravity or to have a constant velocity. If *grav* is set to *False*, then a velocity should be specified at the $v =$… equation. Once all the parameters of the experiment are set, the list of distances to simulate for should be specified. These distances will lie in an array, defined just after the parameters. The first two numbers in the array will specify the ends of the distance range and the third number will specify the number of distances within this range to calculate the distribution at. The larger this third number is, the clearer the resulting visual will be, but it will also take longer for the program to run. Similarly, the range of *x*-values that the program will calculate the distribution at for each distance should be specified the same way. Finally, the distance and range of *x*-values for which the line plot should be created should also be specified at the line plot variables. If the Fraunhofer distribution is also wanted on the line plot, the Fraunhofer variable should be toggled to *True*. If the Fraunhofer distribution is selected, the velocity should also be defined to give the de Broglie wavelength of the particle Once the program is run, the two-dimensional color plot will be produced for the given *x* and *z* ranges, and the line plot will be produced as specified.

Acknowledgements

I would like to thank my advisor, Professor Dante Amidei, for his leading and advising of this project for over a year. His guidance and support have been integral to the success of this project and to my understanding of quantum mechanics and the Feynman Path Integral Method. I would also like to thank him for his suggestions and review of this report in order to improve its presentation of our work.

I would also like to thank the University of Michigan Physics Department for its support and resources during the writing of this thesis. I would like to thank the professors, instructors, graduate students, and staff who have enabled my undergraduate education within the College of Literature, Science, and the Arts, culminating in this thesis. Each experience I have had and class I have taken have increased my knowledge and understanding and allowed me to produce this work.

Finally, I would like to thank my family for providing me with the resources to pursue my undergraduate education at the University of Michigan. I would like to thank both my family and friends for their support over these four years as I have progressed towards earning my degree.

References

[1] Pedrotti, Frank L., et al. *Introduction to Optics*. 3rd ed, Cambridge university press, 2018.

[2] Young, Hugh D., et al. *Sears and Zemansky's University Physics: With Modern Physics*. 14th edition, Pearson, 2016.

[3] Davisson, C., and L. H. Germer. "The Scattering of Electrons by a Single Crystal of Nickel." *Nature*, vol. 119, no. 2998, Apr. 1927, pp. 558–60. *DOI.org (Crossref)*, https://doi.org/10.1038/119558a0.

[4] Jönsson, Claus. "Electron Diffraction at Multiple Slits." *American Journal of Physics*, vol. 42, no. 1, Jan. 1974, pp. 4–11. *DOI.org (Crossref)*, https://doi.org/10.1119/1.1987592.

[5] Merli, P. G., et al. "On the Statistical Aspect of Electron Interference Phenomena." *American Journal of Physics*, vol. 44, no. 3, Mar. 1976, pp. 306–07. *DOI.org (Crossref)*, https://doi.org/10.1119/1.10184.

[6] Bach, Roger, et al. “Controlled Double-Slit Electron Diffraction.” New Journal of Physics, vol. 15, no. 3, Mar. 2013, p. 033018. DOI.org (Crossref), https://doi.org/10.1088/1367-2630/15/3/033018.

[7] Rosa, Rodolfo. “The Merli–Missiroli–Pozzi Two-Slit Electron-Interference Experiment.” *Physics in Perspective*, vol. 14, no. 2, June 2012, pp. 178–95. *DOI.org (Crossref)*, https://doi.org/10.1007/s00016-011-0079-0.

[8] Shimizu, Fujio, et al. “Double-Slit Interference with Ultracold Metastable Neon Atoms.” *Physical Review A*, vol. 46, no. 1, July 1992, pp. R17–20. *DOI.org (Crossref)*, https://doi.org/10.1103/PhysRevA.46.R17.

[9] Feynman, Richard P., and Hibbs, Albert R. *Quantum Mechanics and Path Integrals*. Emended ed, Dover Publications, 2010.

[10] Philippidis, C., Dewdney, C. & Hiley, B.J. Quantum interference and the quantum potential. Nuov Cim B 52, 15–28 (1979). https://doi.org/10.1007/BF02743566

[11] Gondran, Michel, and Gondran, Alexandre. *Numerical Simulation of the Double Slit Interference with Ultracold Atoms*. arXiv:0712.0841, arXiv, 5 Dec. 2007. *arXiv.org*, http://arxiv.org/abs/0712.0841.

[12] Beau, Mathieu. “Feynman Path Integral Approach to Electron Diffraction for One and Two Slits, Analytical Results.” *European Journal of Physics*, vol. 33, no. 5, Sept. 2012, pp. 1023–39. *arXiv.org*, https://doi.org/10.1088/0143-0807/33/5/1023.

[13] Larsen, Stuart. “Sim 9 Double Slit Simulation - Schrodinger FDTD.” C0nrad’s C0rner, 9 Apr. 2022, https://blog.c0nrad.io/posts/sim-9-double-slit-schrodinger-fdtd/.

[14] Mena, Arturo. “Solving the 2D Schrödinger Equation Using the Crank-Nicolson Method.” Quantum Things, 26 Feb. 2021, https://artmenlope.github.io/solving-the-2d-schrodinger-equation-using-the-crank-nicolson-method/.

[15] Griffiths, David, et al. *Introduction to Quantum Mechanics*. 3rd ed, Cambridge University Press, 2018.

[16] Cernak, Daniel. *Path_Integral_Two-Slit_Toolkit*. 15 Apr. 2024, https://github.com/cernakd/Path_Integral_Two-Slit_Toolkit